

## RPC-IES: THE ION AND ELECTRON SENSOR OF THE ROSETTA PLASMA CONSORTIUM

J. L. BURCH<sup>1</sup>, R. GOLDSTEIN<sup>1,\*</sup>, T. E. CRAVENS<sup>2</sup>, W. C. GIBSON<sup>1</sup>, R. N. LUNDIN<sup>3</sup>,  
C. J. POLLOCK<sup>1</sup>, J. D. WINNINGHAM<sup>1</sup> and D. T. YOUNG<sup>1</sup>

<sup>1</sup>*Southwest Research Institute, P.O. Drawer 28510, San Antonio, TX 78228, USA*

<sup>2</sup>*Department of Physics and Astronomy, University of Kansas, Lawrence, KS 66045, USA*

<sup>3</sup>*Swedish Institute of Space Physics, S-98128 Kiruna, Sweden*

(\*Author for correspondence: E-mail: rgoldstein@swri.edu)

(Received 7 February 2006; Accepted in final form 27 June 2006)

**Abstract.** The ion and electron sensor (IES) is part of the Rosetta Plasma Consortium (RPC). The IES consists of two electrostatic plasma analyzers, one each for ions and electrons, which share a common entrance aperture. Each analyzer covers an energy/charge range from 1 eV/e to 22 keV/e with a resolution of 4%. Electrostatic deflection is used at the entrance aperture to achieve a field of view of  $90^\circ \times 360^\circ$  ( $2.8\pi$  sr). Angular resolution is  $5^\circ \times 22.5^\circ$  for electrons and  $5^\circ \times 45^\circ$  for ions with the sector containing the solar wind being further segmented to  $5^\circ \times 5^\circ$ . The three-dimensional plasma distributions obtained by IES will be used to investigate the interaction of the solar wind with asteroids Steins and Lutetia and the coma and nucleus of comet 67P/Churyumov–Gerasimenko (CG). In addition, photoelectron spectra obtained at these bodies will help determine their composition.

**Keywords:** comet 67P/Churyumov–Gerasimenko, solar wind–comet interaction, plasma analyzer, solar wind asteroid interaction

### 1. Introduction

The Rosetta Comet Rendezvous Mission will provide a unique opportunity to study a cometary environment and its interaction with the solar wind over a wide range of distances from the Sun, hence a wide range of activity levels. For example, heliocentric distances near 3 AU will provide an excellent opportunity to determine the basic properties of the nucleus because obscuration by gas and dust will be at a minimum. At the other extreme, the orbital segment near perihelion will be ideal for mapping the many plasma boundaries in the cometary environment. These boundaries are formed by the comet's interaction with the solar wind and processes associated with the cometary tail. Intermediate distances will be ideal for studying the threshold levels of both nucleus activity and the interaction of the coma with the solar wind.

The ion and electron sensor (IES), in conjunction with the other component instruments of the Rosetta Plasma Consortium (RPC; Trotignon *et al.*, 1999), will carry out investigations of (1) the solar wind interaction with the nucleus of comet 67P/Churyumov–Gerasimenko (CG), (2) the processes that govern the composition

and structure of the cometary atmosphere, and (3) the interaction between the solar wind and the cometary atmosphere. In addition to the measurements required for the investigation of the comet/solar wind interaction, the IES will be used to study the interaction between the solar wind and two asteroids (Steins and Lutetia).

The IES consists of two electrostatic analyzers (ESAs), one each for electrons and ions. The charged particle optics for the IES are based on a toroidal “top-hat” ESA geometry that gives maximum aperture area for a given analyzer size (Young *et al.*, 1988) and specifically on the deflection optics of the plasma experiment for planetary exploration (PEPE), which was included on the NASA Deep Space 1 mission (Young *et al.*, 2004). The IES is mounted on a top corner of the Rosetta spacecraft pointed in a direction that would normally view the comet. This location allows the IES to view both the comet and the solar wind under most orbital conditions.

## 2. IES Scientific Objectives

### 2.1. THE COMETARY PLASMA ENVIRONMENT AND SOLAR WIND INTERACTION

The nature of the plasma environment around a cometary nucleus strongly depends on the heliocentric distance of the comet and the resulting gas production rate of the nucleus. Most of our understanding of this environment and of the solar wind interaction with comets comes from information obtained from spacecraft encounters with comets in the mid-1980s: the Giotto, Vega 1 and 2, Suisei, and Sakigake encounters with comet Halley in 1986; and the ICE encounter with comet Giacobini–Zinner in 1985. Further information has since been obtained from the Giotto encounter with comet P/Grigg–Skjellerup in 1992 (e.g., Goldstein *et al.*, 1994).

Figure 1 illustrates two extreme cases of the solar wind interaction with a comet: (a) at large heliospheric distances where the bare nucleus is fully exposed to the solar wind and solar ultraviolet radiation; and (b) a fully developed solar wind interaction for an active comet near perihelion at  $\sim 1$  AU, in which the nucleus and inner coma are shielded from the solar wind by the comet’s own atmosphere and ionosphere.

Cometary gas and dust are produced from only a small fraction of the surface of a nucleus (about 10% for Halley and probably about 1% for less active short period comets). Far from the Sun (heliospheric distances  $d > 3$  AU), the surface is cold, and activity is very low. As the cometary nucleus approaches the Sun and its surface temperature increases, volatiles (mainly water but also CO<sub>2</sub>, etc.) sublime from a portion of the surface and expand into space, forming the cometary coma. Dust particles are carried with the gas flow (Gombosi *et al.*, 1986), so that a dust coma forms. A dust tail also forms as radiation pressure accelerates the dust particles

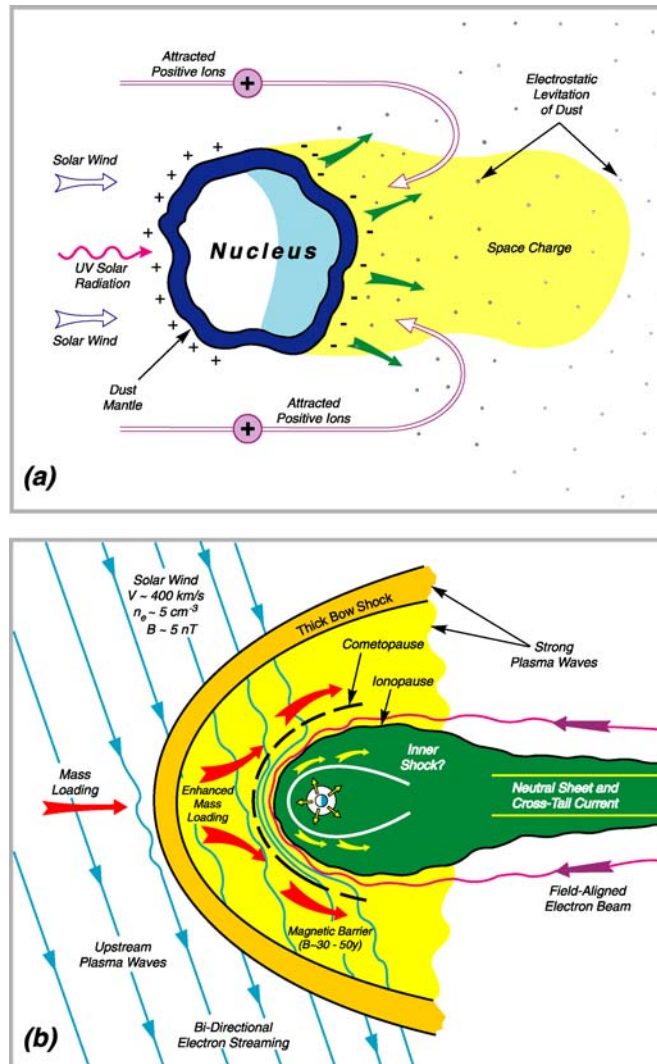


Figure 1. (a) Solar wind interaction with a bare nucleus at large heliospheric distances ( $d > 3$  AU). (b) Plasma environment of an active comet near perihelion (adapted from Flammer, 1991). Key plasma boundaries such as the bow shock, cometopause, and diamagnetic cavity boundary (or contact surface) are shown. Courtesy D. A. Mendis.

anti-sunward. Between about 2 and 3 AU, cometary activity is modest, but near the comet's perihelion ( $d < 2$  AU) activity can be quite high.

Except in the inner coma of an active comet, collisions between solar wind particles and the cometary neutral gas are quite infrequent. But when a cometary neutral (e.g.,  $H_2O$ ,  $CO_2$ , or a photodissociation product such as O) is photoionized by solar extreme ultraviolet (EUV) radiation or charge transfers with a solar wind

proton (Cravens *et al.*, 1987), a cometary ion is created. Initially, this relatively massive newborn ion is almost stationary (i.e., having the neutral outflow speed of about 1 km/s) (Krankowsky *et al.*, 1986). As the ion is accelerated by the electric field of the solar wind, its motion becomes a combination of  $\mathbf{E} \times \mathbf{B}$  drift and gyration. The resulting “pickup ion” (with energy of about 1 keV/amu) also generally drifts along the magnetic field with respect to the solar wind, and the ion distribution function that results is called a ring-beam distribution. Waves in the magnetic field are generated by this ring-beam distribution and tend to scatter the cometary ions, so that their distribution function becomes more isotropic and they are more completely “assimilated” into the solar wind flow.

The heavy cometary ions mass-load and slow down the solar wind and ultimately lead to the formation of a bow shock, magnetic barrier, and magnetic tail (Flammer, 1991). This part of the solar wind interaction with comets is well described by MHD models. For an active enough comet with a dense neutral coma, collisions become important in the inner coma; and charge–exchange collisions can begin to remove the fast solar wind protons from the plasma flow (which is now much slower than the original solar wind speed). This transition happens near a boundary called the cometopause (Cravens, 1991). Inside such a transition, the plasma is mainly of cometary origin and is much colder, slower, and denser than the plasma in the solar wind, with the solar wind electrons penetrating more deeply into the coma than the protons.

## 2.2. ELECTRONS IN THE COMETARY COMA

The electron plasma environment near a comet is a mixture of charged particle populations of solar wind and cometary origin. The ratio and characteristics of this mix change with radial distance from the comet. Electrons of cometary origin are dominated by photochemistry, and the generic cometary electron populations can be viewed as a population of newly formed photoelectrons and Auger electrons in a background of degraded electrons, which have become thermalized through elastic and inelastic collisions. The IES instrument has the capability of making the first high-resolution measurements of cometary photoelectrons, which are needed to confirm the existence of spectral peaks. Knowledge of the individual peaks in the spectrum, when they are not degraded significantly by collisions, allows identification of the parent atoms, either on the nucleus at large heliocentric distances or in the coma at small and medium heliocentric distances.

The background electrons are thermalized to different levels depending on distance from the nucleus. Closer to the comet, where the electrons are strongly coupled to the neutrals, the electron temperature is expected to be close to the neutral temperature (300–500 K), while farther from the nucleus, where the electrons and neutral species are decoupled, the temperature is expected to be higher, i.e., closer to the average photoelectron energy. Where the decoupling occurs is an open question.

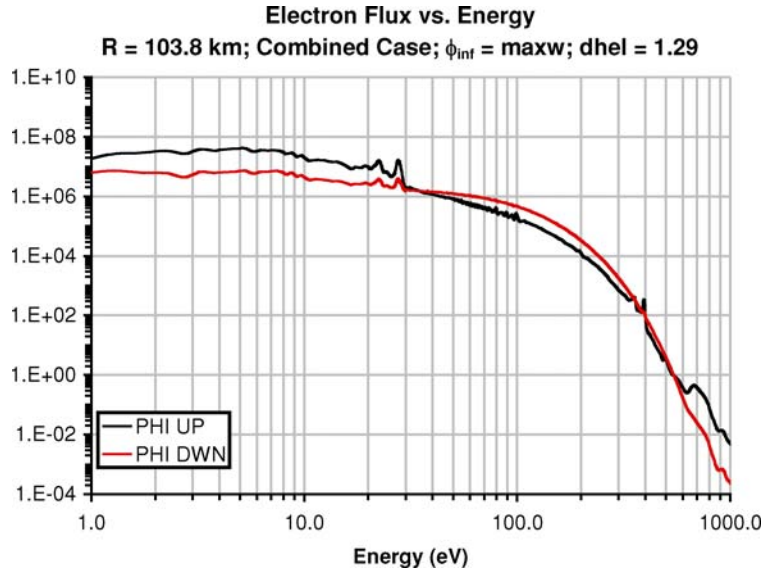


*Figure 2.* Predicted supra-thermal electron fluxes versus energy at a distance of 104 km from the nucleus of comet CG near its perihelion. Fluxes for two directions along the draped interplanetary magnetic field are shown. Both solar wind electrons and photoelectrons associated with ionization of cometary neutrals are included in the calculations. (Spacecraft generated photo electrons are not included.)

By monitoring the electron temperature, we can determine this position and its evolution with activity. A rise in temperature indicates a change in coupling, while the gradient indicates how rapidly this change occurs.

Most of the time, while the spacecraft is in interplanetary space, the electrons measured by IES will be solar wind electrons, which typically have Maxwellian-like distribution functions with thermal energies of several electronvolts to tens of electronvolts. The population of supra-thermal electrons above this energy will also be observable. However, when the comet is within about 2 AU then photoionization of cometary neutrals by solar radiation produces photoelectrons of different energies. Figure 2 shows some model predictions from a two-stream transport code of the electron distribution function for comet CG near perihelion. The photoelectron contribution is most easily distinguished from the solar wind electrons by the discrete structures evident in the electron spectra near 25 eV. (Note that photoelectrons produced by the spacecraft surface are not included here.) The IES 4% energy resolution is more than adequate to resolve these structures, which provide a good diagnostic for the interaction of solar radiation with cometary neutral gas. The methods used to calculate the electron fluxes were described by Gan and Cravens (1990). Some general discussion of electron energetics and thermal balance, including the role of supra-thermal electrons, in cometary plasma environments can be found in several review papers (e.g., Cravens and Gombosi, 2004; Cravens, 1991).

### 2.3. EXPECTED RESULTS

In this section, the expected results of the IES investigation are outlined for three different ranges of heliocentric distance.

- *Large heliocentric distances ( $d > 2$  AU)—direct solar wind interaction with the nucleus.* At large heliocentric distances ( $d > 2$  AU), the comet nucleus is unshielded, and solar wind protons ( $\sim 1$  keV) and electrons ( $\sim 10$  eV) can affect the surface directly. Some energetic cometary pickup ions (tens of kiloelectronvolts) can also affect the surface. The IES will make measurements of these populations that will contribute to understanding four key processes: (1) sputtering and ion implantation, (2) electrical charging of the surface and grains on the surface and in the coma, (3) wake effects, and (4) remanent magnetization of the nucleus.
- *Intermediate heliocentric distances ( $1.5$  AU  $< d < 2$  AU)—weak interaction.* At intermediate heliocentric distances ( $1.5$  AU  $< d < 2$  AU), the nucleus is shielded by the coma from the most energetic solar wind (protons and cometary pickup ions), but a fully thermal plasma environment has yet to develop. The flow speeds and temperatures are still relatively high, and the ion distribution functions still might not be fully Maxwellian. A cometopause and bow shock may be present, along with a rudimentary plasma tail, but a diamagnetic cavity does not exist. The IES will assess the degree of shielding of the nucleus from the solar wind. The IES measurements of the plasma environment (densities, temperatures, and flow velocities) will be used to investigate (1) coma ionization rates, (2) ion gyrofrequency waves, and (3) electrical charging currents of grains and the nucleus.
- *Heliocentric distances near cometary perihelion ( $d < 1.5$  AU)—strong interaction.* At heliocentric distances near cometary perihelion ( $d < 1.5$  AU), the nucleus should be fully shielded, and a sizeable (few hundred kilometer) thermal plasma region should be present, although a diamagnetic cavity still might not form or be only rudimentary. In addition to continuing the investigation of surface charging and ionization rates near perihelion, the IES data acquired during this phase of the mission will be used to investigate (1) predicted reverse shock inside the contact surface, (2) energetic ions in the inner coma, (3) the nature and stability of the contact surface, (4) the nature of the bow shock, (5) the ion gyrofrequency waves, and (6) the velocity and composition of the pickup ions.

### 3. IES Instrument Description

The IES for ROSETTA is an ESA that uses electrostatic angular deflection to obtain a scanned field of view of  $90^\circ \times 360^\circ$ . The objective of the instrument is

TABLE I  
IES parameters.

Parameter	Value
Energy range	1 eV/e to 22 keV/e
Resolution ( $\Delta E/E$ )	0.04
Scan	Mode dependent
Angle range (FOV)	$90^\circ \times 360^\circ$ ( $2.8\pi$ sr)
Resolution (electrons)	$5^\circ \times 22.5^\circ$ (18 azimuthal $\times$ 16 polar)
Resolution (ions)	$5^\circ \times 45^\circ$ (18 azimuthal $\times$ 7 polar) $5^\circ \times 5^\circ$ (18 azimuthal $\times$ 9 polar) (in solar wind direction)
Temporal resolution: 3D distribution	128 s
Downlink data	300 s
Geometric factor: total (ions)	$5 \times 10^{-4}$ cm <sup>2</sup> sr eV/(eV counts/ion)
Per 45° sector (ions)	$6 \times 10^{-5}$ cm <sup>2</sup> sr eV/(eV counts/ion)
Total (electrons)	$5 \times 10^{-4}$ cm <sup>2</sup> sr eV/(eV counts/electron)
Per sector (electrons)	$3 \times 10^{-5}$ cm <sup>2</sup> sr eV/(eV counts/electron)
Mass	1,040 g
Volume	1,297 cm <sup>3</sup>
Dimensions	Sensor: 73 mm diameter $\times$ 101 mm electronics box: 139 mm $\times$ 121 mm $\times$ 64 mm
Power	1,850 mW
Downlink data rate	5–250 bps

to obtain three-dimensional ion and electron distribution functions over the energy range extending from 1 eV/e up to 22 keV/e with a basic time resolution of 128 s. The angular resolution for electrons is  $5^\circ \times 22.5^\circ$  (18 azimuthal by 16 polar-angle sectors. For ions, the angular resolution is  $5^\circ \times 45^\circ$  (18 azimuthal by 7 polar-angle sectors, covering  $315^\circ$  of polar angle) with additional segmentation to  $5^\circ \times 5^\circ$  in the  $45^\circ$  polar-angle sector most likely to contain the solar wind (giving a total of 16 polar-angle sectors for ions). Table I lists the complete set of IES performance parameters and its resource requirements.

### 3.1. PRINCIPLE OF MEASUREMENTS

A cross-sectional view of the IES sensor is shown in Figure 3. The back-to-back top-hat geometry of the IES ESA allows it to analyze both electrons and positive ions with a single entrance aperture. The IES has cylindrical symmetry about the vertical axis passing through its center. The IES top-hat analyzers have toroidal geometry with a smaller radius of curvature in the deflection plane than in the orthogonal plane. This toroidal feature results in a flat deflection-plate geometry

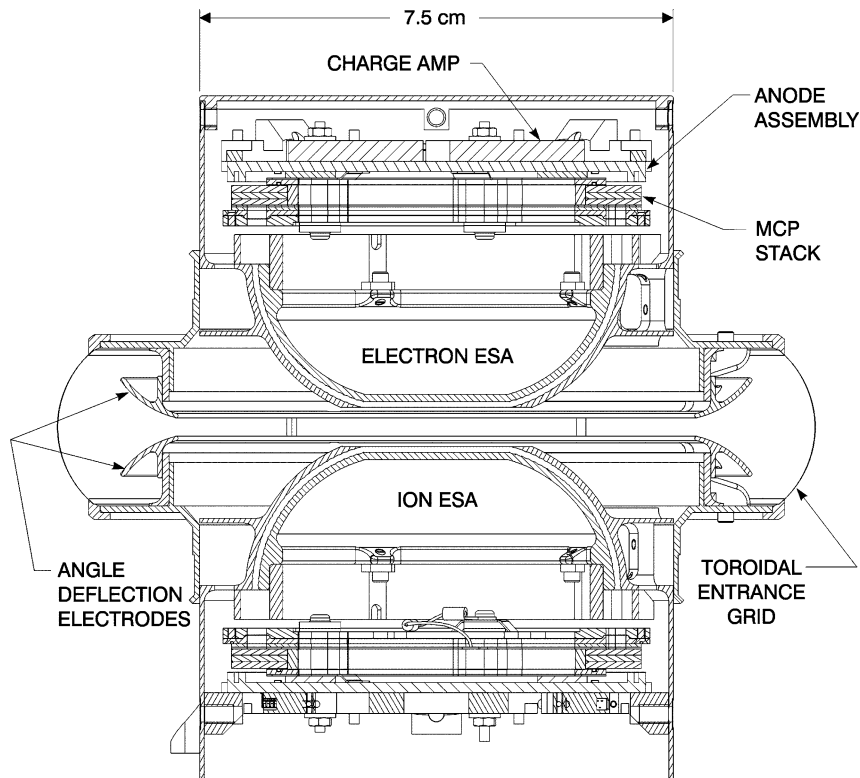
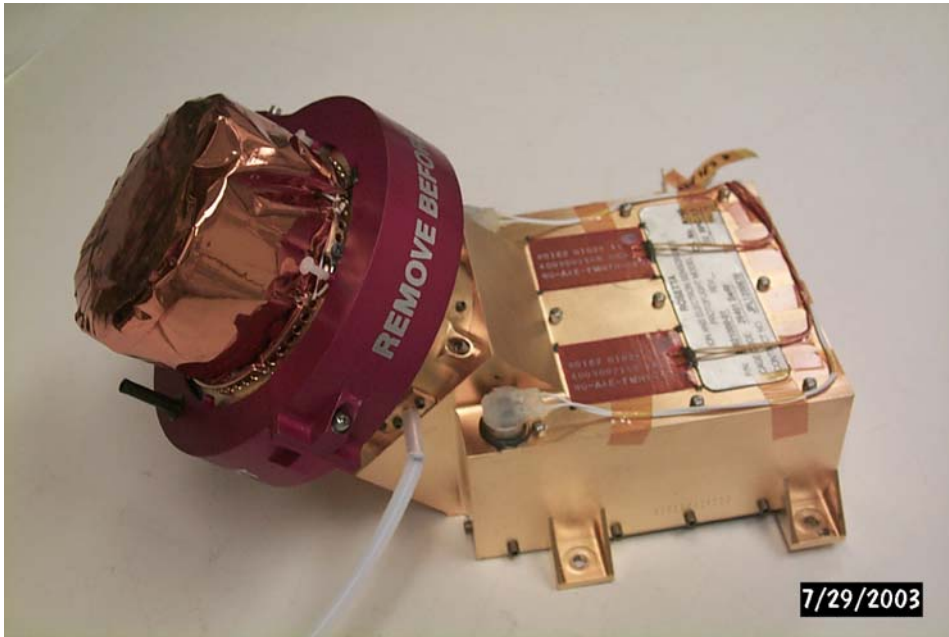


Figure 3. IES ESA. Shaded surfaces lie in a vertical plane through the center of the cylindrically symmetric sensor.

at the poles of the analyzers and has the advantage that the focal point is located outside the analyzers rather than within them, as is the case with spherical top hat analyzers (Young *et al.*, 1988). In addition, the IES entrance aperture contains electrostatic deflection electrodes, which expand its azimuthal angle field of view to  $\pm 45^\circ$ . With the typical top hat polar-angle field of view of  $360^\circ$ , the IES acquires a total solid angle of  $2.8\pi$  sr.

Ions and electrons approaching the IES first encounter a toroidal-shaped grounded grid encircling the instrument aperture (Figure 3). Once inside the grid, the electric field produced by curved bipolar electrodes deflects ions and electrons with an energy- and angle-dependent range of energies and azimuthal angles into a field-free entrance aperture (see Table I for the nominal values of resolution). The particles then enter the top-hat region and the electric field produced by the flat ESA segments of the ion and electron analyzers. Particles within a narrow 4% energy passband will pass through the analyzers and be focused onto microchannel plates (MCPs), which produce charge pulses on the 16 discrete anodes that define the polar acceptance angles.



*Figure 4.* Photograph of completed IES instrument shortly before the integration with the Rosetta spacecraft. The red “Remove before Flight” cover is seen protecting the entrance grid A thermal blanket cap covers the upper portion of the detector assembly.

A photograph of the instrument, taken shortly before integration with the Rosetta spacecraft, is shown in Figure 4.

### 3.2. IES ELECTRONICS

A cross section of the integrated IES sensor and electronics package is shown in Figure 5. The top three electronic boards comprise the high-voltage subsystem, which produces the electron and ion MCP operating voltages, the deflection potentials for the electron and ion ESA, and the voltages for the entrance angle deflection electrodes. The bottom two boards in the electronics enclosure contain the sensor controller circuitry. The main functions of the sensor controller are to control the IES operating modes, acquire real-time data from the sensor, histogram the data, and store it for downloading to the RPC Plasma Interface Unit (PIU) through an IEEE 1355 interface. This circuitry includes an RTX 2010 microprocessor and two field programmable gate arrays. Figure 6 shows a photograph of the assembled system, partially folded open to illustrate the use of a flexible cable to connect the two portions of the instrument. Figure 7 shows a schematic block diagram of the IES electronics.

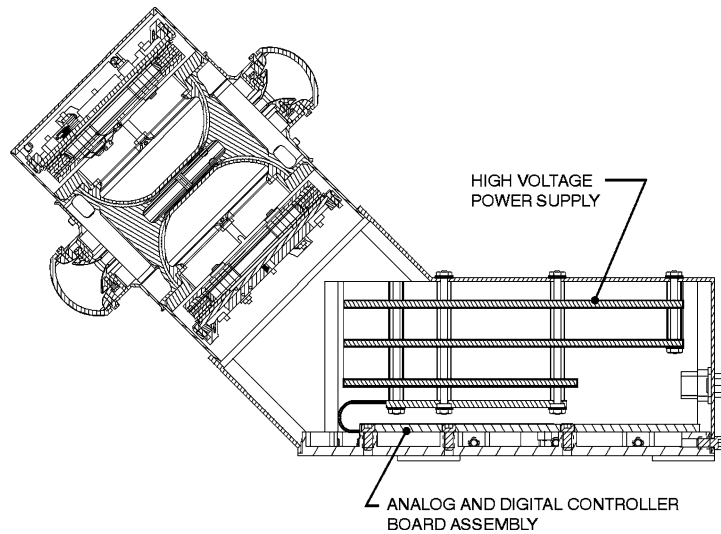


Figure 5. Cross section of the integrated instrument.

### 3.2.1. IES Detectors

*3.2.1.1. Description.* Highly integrated discrete-anode detector assemblies have been developed for IES. A z-stack of annular MCPs is mounted in proximity to each anode. The anode design depends upon species: electrons or ions. Both use a 16-channel discrete approach. The 16 available channels are distributed differently for the two species, which allows for high-resolution solar wind measurements using the ion anode. Electron anode active surfaces operate at high positive voltage and therefore must be capacitatively coupled to the charge amplifier inputs. The anodes are fabricated from multi-layer polyimide printed wiring board. In the case of the electron anode, HV capacitors are built into the printed wiring board. The ion anode couples signals conductively, using connections (vias) through the board. In both cases, the MCP charge pulses are coupled to 16 independent charge amplifier/discriminator pairs. This circuitry is provided by two commercially available Monolithic Octal Charge Amplifier and Discriminator (MOCAD) chips. The MOCADs are mounted on the back of each anode. The electrical interface to each detector requires high voltage for the MCPs, low voltage power for the MOCADs, sixteen digital signal lines carrying digital event pulses, a simple digital stimulator for testing the MOCADS and downstream data system, and associated ground wires.

### 3.2.2. IES Data Handling

The electron and ion data each are acquired at 16 polar angles, 18 azimuthal angles, and 256 contiguous energy levels. The data are stored in compressed form in static random access memory (SRAM) and uploaded to the PIU at an average rate of

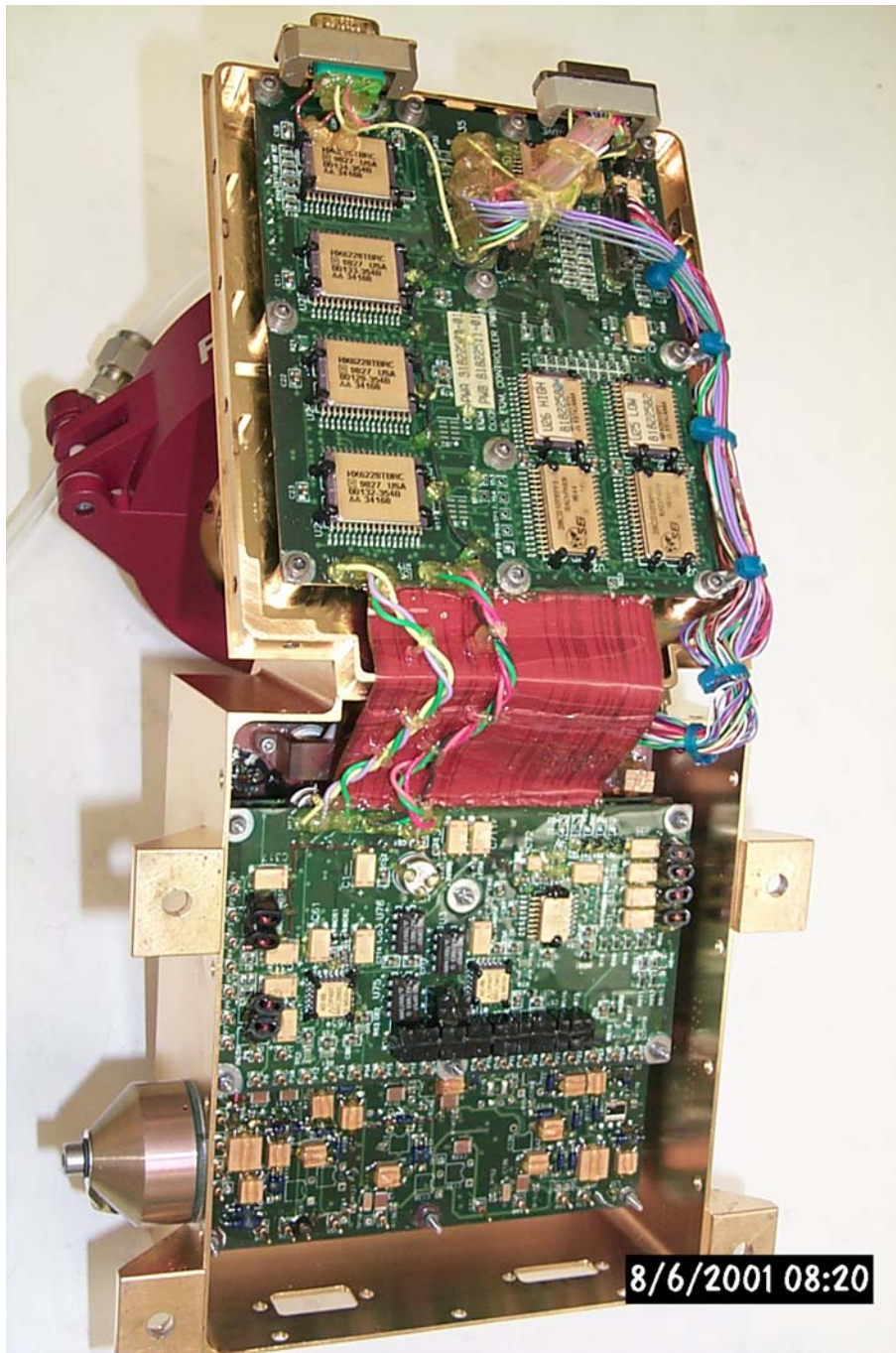


Figure 6. Photograph of completed electronics assembly.

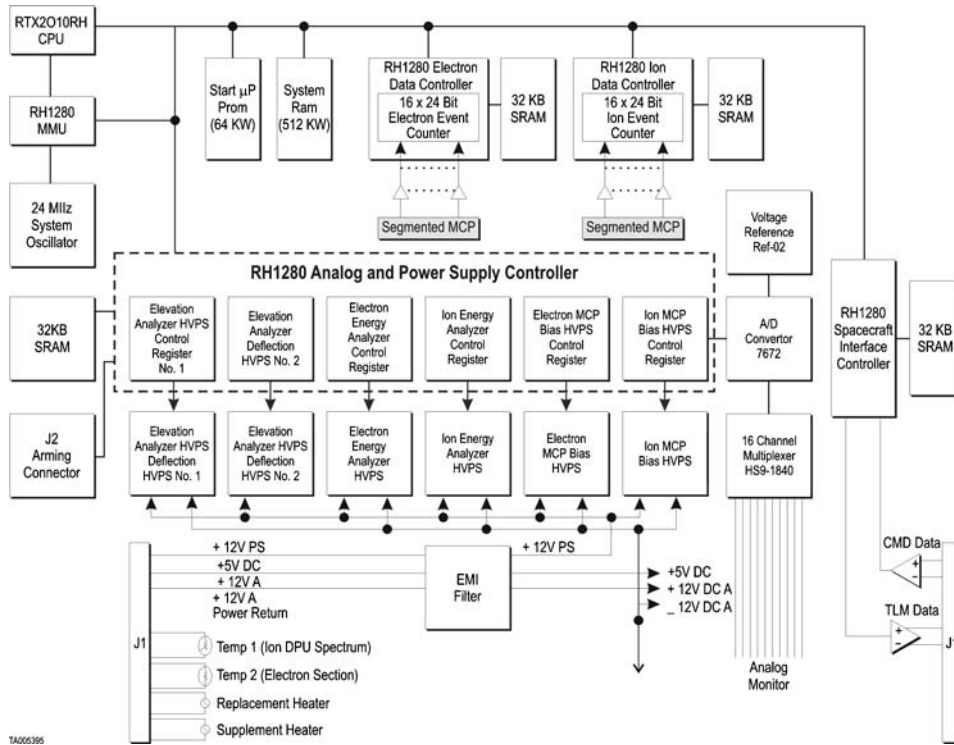


Figure 7. Schematic block diagram of IES electronics.

9,375 bytes every 300 s. The various science modes specify high-voltage levels and stepping sequences on the energy and azimuthal angle ESA. The electron and ion analyzers are stepped together through the same energy levels and azimuthal angles.

#### 4. IES Operational Modes

The IES instrument has several operational modes. The instrument is always brought up first in the initialization mode in order to ensure that all commanded states are in safe, nominal ranges. After initialization, the low-voltage checkout mode is entered, and all low-voltage circuitry completes a self test. Next the high-voltage checkout mode is used to step the high voltages up to operational levels while closely monitoring all currents for nominal operation. Science Mode 1 is a baseline science mode, which provides a comprehensive data set on a default basis. This mode provides a general survey measurement over all energies and angles.

While in Science Mode 1, two different engineering modes can be run in the background in order to monitor different housekeeping functions. From Science

Mode 1, other modes such as the Region-of-Interest Mode, and Snapshot Mode can be entered for focused studies of regions such as the solar wind or the comet and asteroid environments. These modes allow dedicating the energy and angle ranges and resolutions for a specific science objective. If the high-voltage circuitry is turned off, the Low-Voltage Checkout Mode is run before the high voltage is brought up again.

A minimum of elective instrument commanding is planned. The main choices within the realm of science operations involve (1) choosing from a finite selection of pre-defined science data products, and (2) managing the instrument high voltage. The former is controlled by operating from any of a number of on-board stored look-up tables. Internal constraints on operations are imposed by considerations that fall into two categories: those that have an immediate science or data impact and those that have a hardware safety impact. Primary safety-related constraints on operations involve two major elements: (1) HV operation, and (2) MCP current limitation.

## 5. IES Electrical Ground Support Equipment

The IES instrument is supported through an electrical ground support equipment (EGSE) station, which simulates the PIU. The IES EGSE consists of a personal computer (PC), an IEEE 1355 interface card, a digital I/O card, an analog I/O card, and  $\pm 28$  V,  $\pm 12$  V,  $-12$  V, and  $\pm 5$  V power supplies. The EGSE is controlled through a system of menus written to run under LabView. The EGSE provides power to the IES instrument and transmits commands and receives data over the IEEE 1355 serial link. The temperature of the baseplate of the IES instrument is also monitored using the analog I/O card.

## 6. IES Instrument Performance

We show here the selected examples of the IES performance. Figure 8 is a plot illustrating the  $5^\circ$  resolution of the ion “fine” anodes, measured in the Southwest Research Institute calibration chamber. The performance is within the design angular resolution.

During March 2005, the Rosetta spacecraft performed a close flyby of Earth as part of the mission plan. The IES operated for several hours and measured ion and electron fluxes during the flyby. Figures 9 and 10 show spectrograms of the measured electrons and ions, respectively, integrated over all look directions.

Along the abscissa axis in both plots, the time in UTC (Coordinated Universal Time) as well as GSM (Geocentric Solar Magnetospheric) coordinates are given. The ordinate is particle energy, and the particle counts for each of the 128 energy

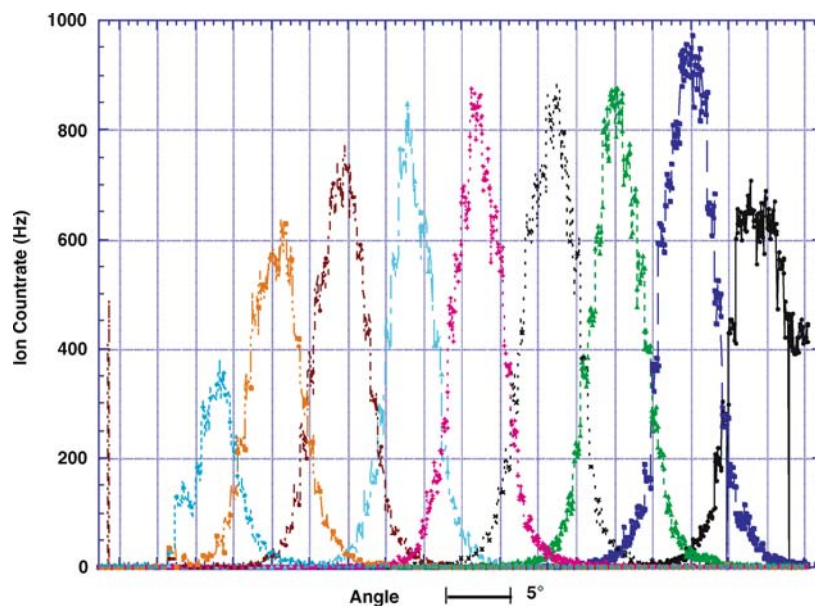


Figure 8. Laboratory calibration measurements showing the 5° resolution of the ion “fine” anodes.

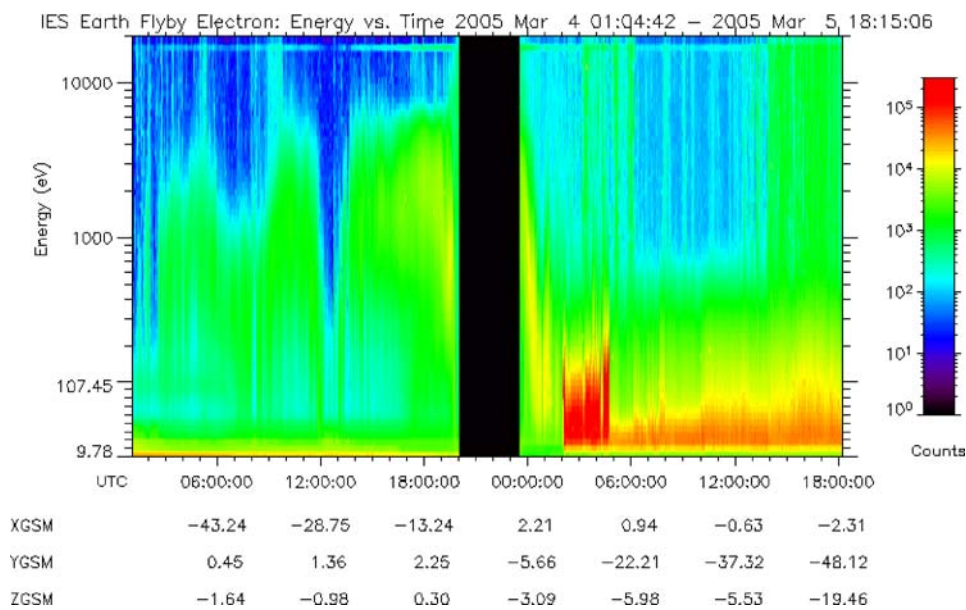


Figure 9. Color spectrogram showing IES-measured electron count rate during the March 2005 Rosetta Earth flyby.

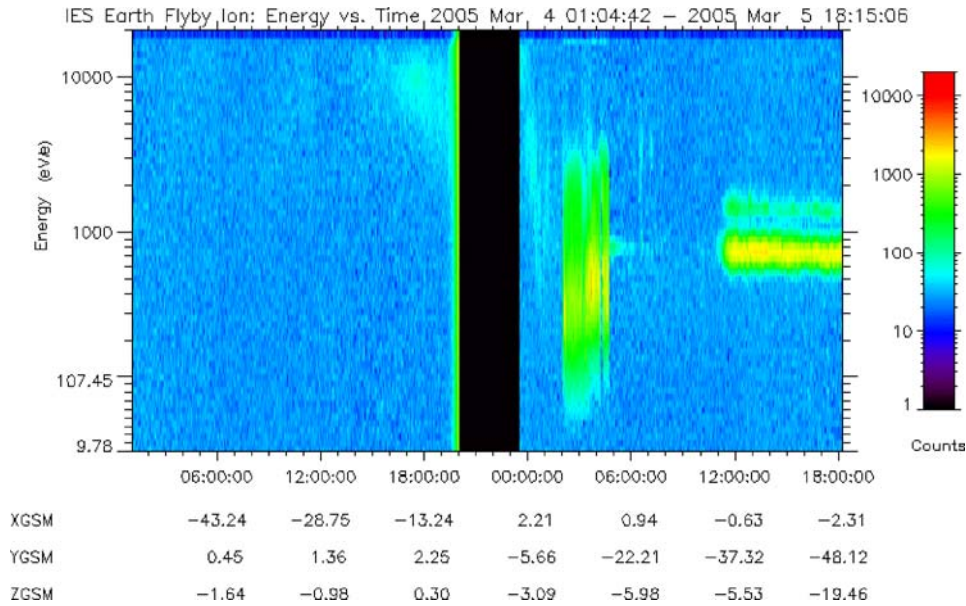


Figure 10. Color spectrogram showing IES-measured ion count rate during the March 2005 Rosetta Earth flyby.

steps is given by the color bar. Beginning on the left, on March 4, Rosetta came up the geotail toward Earth closest approach (CA) shortly before midnight. Earth's magnetosphere was very quiet on the fourth and hence the count rate, especially in the case of the ions, was very low until near CA when a higher flux of energetic particles was encountered. The IES high voltages were turned off during transit of the radiation belts to protect the instrument. After CA, the spacecraft passed through the magnetosheath and bow shock into the solar wind. The solar wind protons and alpha particles are clearly seen in the ion spectrogram after about 12:00 UTC on March 5.

## 7. IES Instrument Summary and Conclusions

As an element of the Rosetta Plasma Consortium, the IES provides three-dimensional plasma distribution functions of electrons and ions over an energy/charge range from 1 eV/e to 22,000 eV/e. Through the use of electrostatic angle scanning, the IES achieves a field of view of  $90^\circ \times 360^\circ$ . The angular resolution for electrons is  $5^\circ \times 22.5^\circ$ , while the angular resolution for ions is  $5^\circ \times 45^\circ$  with one  $45^\circ$  sector further segmented to a resolution of  $5^\circ$  for measurement of the solar wind. The IES instrument is mounted on the spacecraft in such a way as to be able to acquire the comet nucleus, asteroids, and the solar wind for most orbital locations

and attitudes. The IES data will be combined with the fields and particles data from the other RPC instruments to investigate the interaction of the solar wind with the comet and asteroids. The long-term orbital nature of the cometary encounter will allow for the investigation of cometary plasma processes over a wide range of heliocentric distances, which will correspond to a very wide range of cometary activity levels from a nearly quiescent state, in which the solar wind will impact the nucleus directly, to a very active state, in which a well-developed coma, bow shock, and tail will be present.

### Acknowledgments

We thank the many SwRI engineers and technicians for their dedication in the design, fabrication, and testing of IES. The design, development, and operation of IES have been carried out, in part, under funding provided by NASA through a contract with the Jet Propulsion Laboratory, California Institute of Technology.

### References

- Cravens, T. E.: 1991, in Newburn, R. L. Jr., *et al.* (eds.), *Comets in the Post-Halley Era*, Kluwer Academic Publishers, Norwell, MA, p. 1211.
- Cravens, T. E., and Gombosi, T. I.: 2004, *Adv. Space Res.* **33**, 1968.
- Cravens, T. E., Kozyra, J. U., Nagy, A. F., Gombosi, T. I., and Kurtz, M.: 1987, *J. Geophys. Res.* **92**, 7341.
- Flammer, K. R.: 1991, in Newburn, R. L., Jr., *et al.* (eds.), *Comets in the Post-Halley Era*, Vol. 2, Kluwer Academic Publishers, Dordrecht, p. 1125.
- Gan, L., and Cravens, T. E.: 1990, *J. Geophys. Res.* **95**, 6285.
- Goldstein, R., *et al.*: 1994, *J. Geophys. Res.* **19**, 255.
- Gombosi, T. I., Nagy, A. F., and Cravens, T. E.: 1986, *Rev. Geophys.* **24**, 667.
- Krankowsky, D., *et al.*: 1986, *Nature* **321**, 326.
- Trotignon, J. G., *et al.*: 1999, *Adv. Space Res.* **24**(9), 1149.
- Young, D. T., Bame, S. J., Thomsen, M. F., Martin, R. H., Burch, J. L., Marshall, J. A., *et al.*: 1988, *Rev. Sci. Instrum.* **59**, 743.
- Young, D. T., *et al.*: 2004, *Icarus* **167**, 80–88.